KSHV uses viral IL6 to expand infected immunosuppressive macrophages

Michiko Shimoda[1, 2, *], Tomoki Inagaki[1], Ryan R. Davis[3], Alexander Merleev[1], Clifford G. Tepper[2, 4], Emanual Maverakis[1, 2], and Yoshihiro Izumiya[1, 2, 5, *]

[1] Department of Dermatology, School of Medicine, University of California, Davis, Sacramento, CA USA
[2] UC Davis Comprehensive Cancer Center, Sacramento, CA USA
[3] Department of Pathology and Laboratory Medicine, School of Medicine, University of California, Davis, Sacramento, CA USA
[4] Department of Biochemistry and Molecular Medicine, School of Medicine, UC Davis, Sacramento, California USA
[5] Department of Biochemistry and Molecular Medicine, School of Medicine, University of California, Davis, Sacramento, CA USA

*Correspondence:
Michiko Shimoda PhD
Address: UCDMC Research III Room 3100A, 4645 2nd Avenue, Sacramento CA 95817
E. mail: mshimoda@ucdavis.edu
Current Address: Room 310, Building 100, 1001 Potrero Ave, Division of Experimental Medicine, UCSF, San Francisco, CA 94110, USA
E. mail: michiko.shimoda@ucsf.edu
Phone: 628-206-5232

Yoshihiro Izumiya DVM, PhD
Address: UCDMC Research III Room 2200B, 4645 2nd Avenue, Sacramento CA 95817
E. mail: yizumiya@ucdavis.edu
Phone: 916-734-7253

Running Title

KSHV dysregulates monocytes via vIL6

Summary

KSHV causes multiple inflammatory diseases, however, the underlying mechanism is not clear. Shimoda et al. demonstrate that KSHV preferentially infects monocytes and utilizes virally encoded interleukin-6 to expand and deregulate infected monocytes. This helps the virus escape from host immune surveillance.

Abstract

Kaposi's sarcoma-associated herpesvirus (KSHV) is an oncogenic double-stranded DNA virus and the etiologic agent of Kaposi's sarcoma and hyperinflammatory lymphoproliferative disorders. Understanding the mechanism by which KSHV increases the infected cell population is crucial for curing KSHV-associated diseases. Here we demonstrate that KSHV preferentially infects $CD14^+$ monocytes and sustains viral replication through the viral interleukin-6 (vIL6)-mediated activation of STAT1 and 3. Using vIL6-sufficient and vIL6-deficient recombinant KSHV, we demonstrated that vIL6 plays a critical role in promoting the proliferation and differentiation of KSHV-infected monocytes into macrophages. The macrophages derived from vIL6-sufficient KSHV infection showed a distinct transcriptional profile of elevated IFN-pathway activation with immune suppression and were compromised in T-cell stimulation function compared to those from vIL6-deficient KSHV infection or uninfected control. These results highlight a clever strategy, in which KSHV utilizes vIL6 to secure its viral pool by expanding infected dysfunctional macrophages. This mechanism also facilitates KSHV to escape from host immune surveillance and to establish a lifelong infection. 160

Introduction

A virus is an infectious agent that can only replicate within a living host organism. Because of this dependence, viruses have evolved various mechanisms to exploit normal cell functions to escape from host immune surveillance for their survival advantage. This exploitation sometimes associates with prolonged damage to the host leading to pathologic processes and diseases caused by the viral infection (Hoenen and Groseth, 2022).

Kaposi's sarcoma (KS)-associated herpesvirus (KSHV), or human gamma herpesvirus 8 (HHV-8), is an oncogenic double-stranded DNA virus that establishes a lifelong latent infection (Cesarman et al., 2019). KSHV is the etiologic agent of Kaposi's sarcoma and is associated with two lymphoproliferative disorders: multicentric Castleman's disease (MCD) and AIDS-associated primary effusion lymphoma (PEL). KSHV-inflammatory cytokine syndrome (KICS) may also represent a prodromic form of KSHV-MCD, which exhibits elevated KSHV viral loads and circulating inflammatory cytokines including IL-6, IL-10, and a KSHV-encoded IL-6 homolog (vIL-6) (Alomari and Totonchy, 2020; Caro-Vegas et al., 2020; Dumic et al., 2020; Goncalves et al., 2017; Polizzotto et al., 2012; Polizzotto et al., 2016). These highly inflammatory diseases are devastating, and a leading cause of cancer deaths in AIDS patients. Therefore, understanding the mechanism of KSHV infection is crucial for finding a cure for these diseases.

Natural transmission of KSHV most likely occurs through salivary and sexual transmission or during transplantation of KSHV-positive organs into a naïve recipient although initial KSHV infection is normally asymptomatic (Cesarman et al., 2019; Dittmer and Damania, 2019). In experimental settings, KSHV has been shown to infect various types of cell lines and primary cells such as epithelial cells and immune cells that include B cells, monocytes, and dendritic cells through binding to specific cell surface receptors such as Siglec DC-SIGN (Decker et al., 1996; Gregory et al., 2012; Rappocciolo et al., 2006; Staskus et al., 1997; van der Meulen et al., 2021). However, it remains unclear as to whether KSHV may preferentially infect a certain cell type among PBMC. The mechanisms by which KSHV facilitates a lifelong infection by increasing viral reservoirs and impacts the host immune system are also not entirely clear.

KSHV-encoded viral interleukin-6 (vIL6) is a homolog of human interleukin-6, which is encoded by KSHV ORF-K2 and is highly expressed during the lytic replication cycle (Sakakibara and Tosato, 2011). Viral IL6 is also expressed at physiologically functional levels in latently infected cells

92 (Chandriani and Ganem, 2010) and is detectable in the sera and/or tumor tissues of patients with KS,
93 PEL, and MCD (Aoki et al., 2001). Viral IL6 enhances cell proliferation, endothelial cell migration,
94 and angiogenesis, leading to tumorigenesis, and has been suggested to be a driver of KICS (Giffin et
95 al., 2015; Zhu et al., 2014). In addition, vIL6 transgenic mice develop IL6-dependent MCD-like disease
96 (Suthaus et al., 2012) and supported tumor metastasis in a murine xenograft model (Fullwood et al.,
97 2018). Mechanistically, vIL6 directly binds to the gp130 subunit of the IL6 receptor without the need
98 of the IL6 receptor, α, and actives the JAK/STAT pathway to induce STAT3 phosphorylation and
99 acetylation (Alomari and Totonchy, 2020; Cojohari et al., 2020; Molden et al., 1997). In addition, vIL6
100 activates the AKT pathway to promote numerous oncogenic phenotypes (Giffin et al., 2015; Morris et
101 al., 2008; Morris et al., 2012; Zhu et al., 2014). STAT3 activation by vIL6 also increases the VEGF
102 expression through the downregulating caveolin 1 (Alomari and Totonchy, 2020) and promotes
103 angiogenesis, suggesting that vIL6 plays an important role in tumorigenesis through STAT activation.
104 Given that the prototypical human IL6 plays a critical role in immune regulation and inflammation,
105 vIL6 is thought to play a pivotal role in inflammatory KSHV diseases. Here we reveal the role of vIL6
106 in the regulation of monocytes by utilizing recombinant KSHV and de novo infection to the peripheral
107 blood mononuclear cells.
108
109

110 **Results and Discussion**

111

112 **KSHV preferentially infects CD14+ monocytes among PBMC and triggers an inflammatory**
113 **response and macrophage differentiation.**

114

115 To study cell type-specific KSHV infection, we employed a single cell (sc)RNA-seq analysis approach.
116 Recombinant KSHV (rKSHV.219) virions were purified by two serial ultracentrifugations from the
117 culture supernatant of the iSLK.219 cell line, an inducible recombinant KSHV producer. Peripheral
118 blood mononuclear cells (PBMCs) were infected with rKSHV.219 at MOI=1, fixed at various time
119 points (day 0, 1, 2, and 4) after infection, and subjected to scRNA-seq analysis. KSHV infection and lytic
120 replication in single cells were then monitored by the expression of K2 that encodes vIL6.

121 As shown in Fig. 1A, unsupervised, Uniform Manifold Approximation and Projection (UMAP)
122 for dimension reduction analysis identified 9 clusters among peripheral blood mononuclear cells
123 (PBMCs), each of which can be associated with known immune cell subsets based on corresponding
124 lineage-specific gene expression. Thus, *KLRD1(CD94), CD14, APOBEC3A, VMO1, CD79A*, and *CD3E*
125 genes were used as a marker for NK cells, monocytes, intermediate monocytes, non-classical monocytes,
126 B cells, and T cells, respectively, based on the immune cell data available from the Human Protein Atlas
127 (Uhlen et al., 2019). As shown in Fig. 1B, *de novo* KSHV infection of PBMCs in conjunction with
128 scRNA-seq analysis at 1-day post-infection (dpi) revealed that K2 (vIL6) expression was almost
129 completely overlapped with CD14 expression. It should be noted that scant K2 expression was also found
130 in *CD79A*$^+$ B cells, *KLRD1*$^+$ NK and *CD3E*$^+$ T cell clusters. KSHV has been shown to establish latent
131 infection in B cells, causing B-cell lymphoma (Cesarman et al., 2019). However, the correlation in
132 expression of CD14 and K2 was highly significant (p=8e-191) compared to that of CD19 and K2
133 (p=0.065) at 1 dpi. The following kinetic scRNA-seq analysis also showed that K2 and CD14 gene
134 expression were colocalized during 1 to 4 dpi (Fig. 1C). In this experiment, the culture medium was not
135 replenished during the period. Infectious KSHV virions that remained in the culture or were newly
136 released from infected cells could have infected other cell subsets of PBMC besides CD14$^+$ monocytes.
137 Thus, KSHV selectively infects CD14$^+$ monocytes and monocytes can support KSHV lytic
138 replication along with vIL6 gene expression. The kinetic scRNA-seq analysis also revealed that
139 KSHV infection in CD14$^+$ monocytes triggered the activation and inflammatory response immediately
140 after KSHV infection at 1dpi as evidenced by the upregulation of *IL3RA* (CD123), *CCL2*, and *TNFα*

141 (Fig. 1C). The latter was followed by the expression of genes associated with differentiation of M2-like
142 macrophages with a suppressive phenotype (*CD274/PD-L1*, *C1QA*, *RNASE1*, *IL-10*, and *CD163*) during
143 2-4 dpi (Fig. 1D). Collectively, scRNA-seq analysis demonstrates that KSHV preferentially infects
144 $CD14^+$ monocytes among PBMCs and triggers a monocyte inflammatory response followed by a
145 macrophage differentiation program.
146
147
148 **KSHV infection of PBMC triggers STAT activation in dendritic cells and myeloid cell lineages.**
149
150 As a counterpart of the pleiotropic cytokine human IL6, viral IL6 has been shown to exhibit
151 multifunctional pathologic roles in KS diseases (Sakakibara and Tosato, 2011). Therefore, we next
152 studied the role of vIL6 in monocyte activation and differentiation using a *de novo* PBMC infection
153 model. To this end, we generated recombinant KSHV lacking vIL6 expression by inserting stop codons
154 in vIL6 (vIL6STOP) using the KSHV BAC clone BAC16. We also generated a revertant KSHV with
155 intact vIL6 expression (vIL6REV) by changing the sequence back to the original wild-type sequence
156 with BAC recombination. The lack of vIL6 expression in vIL6STOP was confirmed by Western blotting
157 using a monoclonal antibody against vIL6 (a kind gift from Dr. Robert Yarchoan, NIH) (SFig. 1A).
158 First, to evaluate the signaling events triggered by KSHV infection in immune cells, PBMC from
159 healthy donors (n=6, 3 males and 3 females) were infected with vIL6REV (with vIL6 expression) or
160 vIL6STOP (without vIL6 expression) (MOI=1), or mock-infected (PBS). At 1 dpi, cells were fixed and
161 subjected to CyTOF analysis using a 27-color signaling panel that can differentiate 25 immune cell
162 subsets (SFig. 2). The expression levels of 10 signaling molecules were then determined in order to
163 evaluate the early signaling events in PBMCs upon KSHV infection.
164 Unsupervised t-distributed stochastic neighbor embedding (tSNE) for dimension reduction
165 analysis was applied for each infection group. As shown in Fig. 2A, immune cell subsets were clustered
166 based on each marker expression, and the phenotypic changes induced by infection were visualized and
167 identified by comparison between vIL6STOP, vIL6REV, and the mock-infected (PBS) control group
168 (Fig.2 B). The landscape of immune cell phenotypes visualized by the tSNE cell clustering was
169 remarkably similar between the vIL6STOP and vIL6REV infection group, indicating that the anti-viral
170 response was equally triggered in monocytes in vIL6STOP and vIL6-REV infection. Nonetheless, the
171 tSNE visualization revealed that the phenotype of three immune cell populations corresponding to

172 $CD4^+CD3^+$, $CD19^+CD20^-$, and $CD123^+CD14^+$ clusters as indicated in Fig. 2B was different between the
173 infected groups and the mock-infected control group. The $CD123^+CD14^+$ cluster contains a heterogenous
174 cellular population that also expresses CD11c, CD16, and HLA-DR (Fig. 2A). Given that the scRNA-
175 seq results showed preferential KSHV infection in the $CD14^+$ cell population in association with *CD123*
176 (IL3R) upregulation (Fig. 1C), we considered that the changes observed in the $CD123^+CD14^+$ cluster
177 represent the host cell anti-virus response in monocytes after KSHV infection. Changes in $CD4^+CD3^+$
178 and $CD19^+CD20^-$ clusters could be the result of infection and/or indirect activation such as through
179 cytokine production from PBMCs in response to KSHV infection.

180 To evaluate signaling events in detail, we next used a knowledge-based analysis and identified
181 25 immune cell subsets based on the gating described in SFig.2. The activation status of each signaling
182 molecule was evaluated among plasmacytoid dendritic cells (pDC) and monocytic cell subsets including
183 $CD123^+CD11c^+$ cells, myeloid (m)DC, $CD14^{lo}CD16^+$ non-classical monocytes, $CD14^+CD16^+$
184 intermediate monocytes, and $CD14^-CD16^+$ classical monocytes (SFig.2), based on the fold change in the
185 CyTOF signal intensity for infected groups compared to the mock-infected (PBS) control group (Fig. 2C
186 and D). As expected, many of the 10 signaling molecules including STAT1, IKB, and phosphor-PLCγ
187 were strongly upregulated in pDC (Fig. 2C), an immune cell subset responsible for the anti-viral
188 response. Among $CD11c^+$ DC subsets, STAT1 and phospho-STAT3 were the two most significantly
189 activated pathways in $CD123^+CD11c^+$ cells, and less so in myeloid (m)DC (Fig. 2C and D). Among
190 monocyte subsets, STAT1, phospho-STAT3, and pS6 were upregulated after infection (Fig. 2C and D).
191 Consistent with the tSNE results, the activation profiles of 10 signaling molecules in pDC, DC, and
192 monocytes were identical between vIL6STOP and vIL6REV infection (Fig. 2C and D). Thus, at 1dpi
193 both vIL6STOP and vIL6REV viruses triggered indistinguishable host responses in pDC, DCs, and
194 monocytes.

195 In association with upregulation of STAT 1 (Fig. 2C and D), the frequency of the pDCs among
196 dendritic cells at 1dpi increased by infection regardless of the vIL6 expression (Fig. 2E) while the change
197 in the frequency was not significant for $CD123^+CD11c^+$ cells. The frequency of the $CD14^+CD16^+$
198 population also increased by infection in the presence of vIL6 expression in KSHV (Fig. 2E). The vIL6-
199 dependent response suggests a biological role of vIL6 in the activation of infected $CD14^+CD16^+$
200 monocytes.
201
202

203 **KSHV infection promotes activation and proliferation of CD14+ monocytes in a manner**
204 **dependent on vIL-6.**
205
206 To further study the biological significance of vIL6 expression and STAT 1 and 3 activation, monocytes
207 were isolated from PBMCs (n=6) using a magnetic beads-based negative enrichment method and
208 infected with vIL6STOP or vIL6REV KSHV (MOI=1). The viability and phenotype were then analyzed
209 by flow cytometry at 2 dpi. We found that total cell viability (Fig. 3A) and the frequency of activated
210 CD274 (PDL-1) $^{+}$ cells (Fig. 3C) were significantly increased by KSHV infection regardless of the
211 expression of vIL6. These results were expected based on the CyTOF signaling analysis results that
212 demonstrate that the initial host response against vIL6REV and vIL6STOP infection was
213 indistinguishable. As shown in Fig. 1, KSHV infection promptly induced inflammatory cytokine
214 expression in monocytes. Inflammatory cytokines such as TNFα produced by activated monocytes can
215 support their survival in an autocrine manner during the inflammatory response (Wolf et al., 2017).
216 Therefore, it is possible that the effect of vIL6 on cell survival, if any, could be overridden by the effect
217 of other inflammatory cytokines during the early host anti-viral response against KSHV.
218 On the other hand, the frequency of Ki67^{+} proliferating cells and that of CD16^{+} cells were
219 significantly increased in a manner dependent on the presence of vIL6 (Fig. 3B and C). In monocyte
220 cultures, larger and more frequent proliferating blast cells were observed in response to vIL6REV
221 infection compared to that of vIL6STOP infection (Fig. 3D). Intracellular staining of monocytes also
222 confirmed that the frequency of pSTAT1 and pSTAT3 in monocytes was higher in vIL6REV-infection
223 compared to that in vIL6STOP or mock-infection (Fig. 3E). These results collectively suggest that vIL6
224 expression during the early KSHV infection increases the proliferation of infected monocytes via STAT
225 1 and 3 activation. The cellular environment in monocytes may have a unique role in sustaining STAT
226 activation with KSHV infection.
227
228 **KSHV infection changes the transcriptional landscape of macrophages in a manner dependent on**
229 **vIL6 expression.**
230
231 To reveal the biological effect of vIL6 expression in infected monocytes, we next conducted a
232 transcriptomic analysis of *de novo* infected monocytes. To this end, total RNA was isolated from
233 monocytes harvested 7 days post KSHV infection and RNA-seq was performed (Fig. 4A in the

234 Left panel). By 7 days post-infection, the recovery of vIL6REV-infected monocytes was higher
235 than vIL6STOP-infected monocytes as shown later in Fig. 5A because of the increased Ki67^{+}
236 proliferative responses (Fig. 3B and C). Principal component analysis (PCA) demonstrated
237 markedly distinct transcriptional profiles between vIL6REV-infected and vIL6STOP-infected
238 monocytes (Fig. 4A, the Right panel). Volcano plots depict the higher numbers of differentially
239 regulated genes in vIL6REV-infected monocytes (Fig. 4B; e.g., relative to PBS control). To our
240 surprise, vIL6STOP infection had little impact on the transcriptional landscape of monocytes by
241 7dpi, suggesting that vIL6 expression is needed for either sustaining cell signaling activation or
242 maintaining KSHV lytic replication. Those two functions of vIL6 are likely to be mutually
243 exclusive.
244 Among the genes differentially expressed between vIL6REV vs vIL6STOP infection,
245 interferon-induced genes such as *IFITM2*, and *IFITM3*, are substantially upregulated in response
246 to vIL6REV infection (Fig.4B, Top panel). Consistently, Gene Set Enrichment Analysis (GSEA)
247 also revealed that genes associated with host anti-viral innate responses were enriched in vIL6REV
248 infection (Fig. 4C, SFig. 3), while the pathways involving in antigen processing and presentation
249 were downregulated in vIL6REV (Fig. 4D, SFig. 3). While we expected to see upregulation of
250 IFN-related genes in KSHV infected cells, down-regulation of MHC class II genes are unexpected.
251 Representative upregulated IFN-inducible genes and down-regulation of MHC-II were visualized
252 in the heatmap (Fig. 4E). To identify the putative transcription factors that are responsible for
253 vIL6-driven gene regulation, we examined transcription factors that are enriched on promoter
254 regions of differentially transcribed genes. As shown in Fig. 4F, interferon regulatory factors,
255 STAT1 and STAT2 were found as putative transcription factors that are responsible for driving
256 vIL6-associated phenotypes.
257
258 **KSHV infection generates macrophages with an immunosuppressive phenotype in a manner**
259 **dependent on vIL6 expression.**
260
261 Following the transcriptomic study that demonstrated transcriptional landscape changes in KSHV-
262 infected macrophages, we next confirmed functional changes induced in monocytes after KSHV *de*
263 *novo* infection on 7-14 dpi.

264 As shown above, in Fig. 1D, the M2-like macrophage differentiation program had been
265 triggered by 4 dpi. Consistent with this, monocytes in cultures possessed features indicative of
266 macrophages, such as being predominantly of large cellularity with higher FSC and SSC, as shown in
267 Fig. 5A. Also, the recovery of cells was significantly increased in vIL6-REV infection compared to
268 vIL6-STOP infection at 7-14 dpi. Consistent with the transcriptomic analysis in Fig. 4D, the
269 macrophages derived from vIL6-REV infection (vIL6-REV Mac) expressed lower levels of HLA-DR
270 with higher levels of CD16 compared to control groups (Fig. 5B). To test the direct effect of vIL6 in
271 such phenotypic changes, we generated functional recombinant vIL6 capable of activating STAT1
272 (SFig. 1B and C). Monocytes were cultured in the presence of vIL6 (200 ng/ml in serum-free medium)
273 for 9 days, and the phenotype was analyzed by flow cytometry. As shown in Fig. 5C, the overall
274 monocyte viability was increased from 20% to 59% in the presence of vIL6. In addition, monocytes
275 recovered from the 9 days culture showed a trend of reduced HLA-DR expression (Fig. 5D) compared
276 to monocytes cultured without vIL6 (PBS). The results suggested that vIL6 treatment alone could
277 induce phenotypic changes similar to vIL6REV infection.
278 Finally, to evaluate T cell co-stimulatory capacity, CSFE-labeled allogeneic T cells were
279 cultured with macrophages derived from monocytes mock-infected or infected with vIL6REV or
280 vIL6STOP. T cell proliferation was then evaluated as CSFE-dilution by flow cytometry (Fig. 5E, Top
281 panel) in the presence or absence of anti-CD3 stimulation, and with the T cell culture with anti-
282 CD3/CD28 tetramer stimulation as a positive control. As shown in Fig. 5E and summarized in Fig. 5F,
283 the frequency of CFSE-negative proliferated T cells was significantly reduced in co-culture with
284 macrophages from vIL6REV infection (18.5%) compared with uninfected (50.8%) or vIL6STOP-
285 infection groups (78.6%) in the presence of anti-CD3 stimulation. Similar results were found in the
286 cultures without anti-CD3 stimulation with the exception that the extent of T cell proliferation was
287 smaller. These observations are consistent with the transcriptional analysis in Fig. 4, which collectively
288 demonstrates that sustained vIL6-driven KSHV-lytic infection and continuous host anti-viral response
289 in infected monocytes induces an immune suppressive phenotype in differentiating macrophages.
290 Monocytes play a key role in early infections by producing inflammatory cytokines and
291 differentiating into subtypes that play distinct roles in the induction or resolution of inflammation
292 (Watanabe et al., 2019)(Kapellos et al., 2019). Upon activation, some monocytes upregulate CD16
293 (FcgRIII), giving rise to $CD14^{+}CD16^{+}$ intermediate monocytes and $CD14^{-}CD16^{+}$ non-classical
294 monocytes, with a prolonged circulating lifespan. These $CD16^{+}$ monocytes normally exhibit high HLA-

295 DR expression for the capability of antigen presentation, transendothelial migration, and FcR-mediated
296 phagocytosis for anti-viral response (Yeap et al., 2016). $CD16^+$ monocytes also express the highest levels
297 of TNFR2 (CD120b) (Hijdra et al., 2012), which can upregulate the anti-inflammatory cytokine IL-10
298 cytokine (Gane et al., 2016) and supports either cell survival or death (Webster and Vucic, 2020). In this
299 context, we observed an increase in $CD14^+CD16^+$ cells during early *de novo* KSHV infection (Fig.2E
300 and 3B). We speculate that KSHV infects $CD14^+CD16^+$ monocytes by exploiting their FcR- and
301 complement-mediated phagocytosis mechanism and expands them. The vIL6-driven sustained STAT1/3
302 activation may provide infected monocytes with a proliferative advantage over uninfected cells to
303 increase their population size. Furthermore, vIL6-driven lytic infection constitutively triggers host anti-
304 viral responses such as IFN-pathway activation, which in turn, induces regulatory mechanisms (McNab
305 et al., 2015). In the case of *Mycobacterium*-infected macrophages, Type-I IFN signaling decreases energy
306 metabolism (i.e. glycolysis and mitochondrial functions) (Olson et al., 2021) and causes cell death (Zhang
307 et al., 2021). In *Listeria*-infected macrophages, stress-induced p38 mitogen-activated protein kinases
308 (MAPK) signaling synergistically enhances IFN-stimulated genes (ISGs). In macrophages, IL-10
309 production as a part of the IFN-induced regulatory mechanism has been shown to dampen the capability
310 of T cell activation and antigen presentation (McNab et al., 2014; Redpath et al., 1999; Zdrenghea et al.,
311 2015). We show that the induction of a suppressive M2-like macrophage gene program was induced as
312 early as 4 dpi in our scRNA analysis (Fig. 1). Consistent with this, earlier studies by other researchers
313 also showed that KSHV infection and STAT3 activation induce a suppressive phenotype in dendritic
314 cells and the THP-1 cell line (Bhaskaran et al., 2017; Campbell et al., 2014; Gilardini Montani et al.,
315 2020; Qin et al., 2010). Accumulation of such immunosuppressive macrophages may increase the risk
316 of secondary infection or cause chronic infection and inflammation in the host by dysregulating immune
317 responses; this mechanism may increase the risk of KSHV-associated disease development.

318 In summary, this study demonstrates the preferential KSHV infection of monocytes and
319 highlights the critical role of vIL6 in expanding infected monocytes that facilitate a long-term virus
320 reservoir. Similar hijacking strategies to exploit monocyte development and functions have been also
321 reported in Cytomegalovirus (Baasch et al., 2021; Baasch et al., 2020; Cojohari et al., 2020; Shnayder et
322 al., 2020). The current study was unique in that vIL6STOP and vIL6REV rKSHV infection system was
323 introduced to delineate the role of vIL6 from that of the other KSHV-encoded multifunctional factors;
324 however, this study does not clarify whether vIL6 is directly involved as a driver in the expression of
325 ISGs under the host defense program in infected monocytes. Nonetheless, vIL6 was required for the

326 sustaining KSHV lytic infection in monocytes. As shown in Fig.4, in the absence of vIL6, KSHV
327 infection in monocytes generated macrophages indistinguishable with those from uninfected monocytes.
328 In this context, our study suggests that vIL6 and monocytes/macrophages are important therapeutic
329 targets in KSHV-associated diseases. Understanding the mechanism in which vIL6 overcomes the IFN-
330 induced regulatory mechanism and promotes cell proliferation would help develop therapies for KSHV
331 infection. It is also important to determine whether KSHV establishes latent infection in macrophages to
332 facilitate a life-long viral reservoir in patient samples. Of note, KSHV is found in circulating monocytes
333 and macrophages (Decker et al., 1996; Rappocciolo et al., 2006), and blood-derived KS-like spindle cells
334 were found to express macrophage markers (Uccini et al., 1997). Future studies are needed to investigate
335 the possible role of monocytes/macrophages as a long-term viral reservoir in patients with KSHV-
336 associated diseases. (16894w/o space)

337 **Materials and Methods**

338

339 **Cells.** LRCs from healthy donors were purchased from Vitalant. PBMCs were prepared by a standard
340 Ficoll gradient method. PBMCs with a 10-30% range of $CD14^+$ monocytes content measured by flow
341 cytometry were stored in liquid N2 and used for experiments. PBMCs were thawed in warm media,
342 washed twice, counted with the Countess automated cell counter (ThermoFisher), and
343 resuspended at 2-5x10^6 viable cells/ml. Monocytes were isolated with EasySep™ Human monocyte
344 isolation kit (STEMCELL) according to the manufacturer's protocol. PBMCs and $CD14^+$ monocytes
345 were cultured in RPMI1640 medium containing 10% FBS plus antibiotics (2-5 x 10^6 cells/ml,
346 200uL/well in a 96 well plate, 400uL/well in a 48 well plate, or 1ml/well in a 24 well plate) supplemented
347 with or without stimuli for various time as described in each figure legend.

348

349 **Virus preparation.** Doxycycline-inducible rKSHV.219 producer iSLK.219 cell lines were maintained
350 in DMEM supplemented with 10% FBS, 1% penicillin-streptomycin-L-glutamine solution, 10
351 μg/mL puromycin, 400 μg/mL hygromycin B, and 250 μg/mL G418. For virus preparation,
352 iSLK.219 cell lines were stimulated with 0.3 mM Sodium Butylate and 1 μg/ml Doxycycline for 5 days.
353 Recombinant KSHV particles were then purified after two serial ultracentrifugation steps from the
354 culture supernatant of activated iSLK.219 cell lines. Briefly, the culture supernatant was centrifuged
355 at 300 × g for 10 min, and then passed through a 0.8-μm filter to remove cellular debris, and then
356 viral particles were concentrated by ultracentrifugation at 25,000 rpm for 2 hrs at 4°C with a
357 Beckman SW28 rotor. The viral precipitates were resuspended in 500 μL of DMEM along with
358 the residual ~500 μL media in the centrifuge tube and stored at −80°C until use.

359

360 **Quantification of viral copy number**. Two hundred microliters of cell culture supernatant were
361 treated with DNase I (12 μg/mL) for 15 min at room temperature to degrade unencapsidated
362 DNA. This reaction was stopped by the addition of EDTA to 5 mM followed by heating at 70°C
363 for 15 min. Viral genomic DNA was purified using the QIAamp DNA Mini Kit according to the
364 manufacturer's protocol and eluted in 100 μL of buffer AE. Four microliters of the eluate were
365 used for real-time qPCR to determine viral copy number, as described previously (Izumiya et al.,
366 2009).

367

368 **Recombinant KSHV**. To test the role of vIL6, rKSHV.219 lacking vIL6 protein expression
369 (vIL6STOP) was generated by adding stop codons in the vIL6 reading frame with BAC16 (vIL6STOP).
370 We also generated a revertant rKSHV.219 with vIL6 protein expression (vIL6REV) by changing the
371 sequence of vIL6STOP back to the original wildtype sequence with BAC-recombination.
372
373 **KSHV *de novo* infection.** KSHV infection was conducted at MOI=1. Briefly, PBMCs or monocytes (1-
374 2 x 10^6 cells) were suspended in RPMI 1640 medium containing 10% intact FBS (not heat inactivated)
375 supplemented with 8 ug/ml polybrene, and an appropriate amount of rKSHV.219 in PBS (less than 10%
376 of total volume) or PBS alone (i.e., as mock infection) was added to the culture. Cells were kept in the
377 same culture medium until analysis.
378
379 **Single-cell RNA-seq.** 2 x 10^6 PBMCs were infected with rKSHV.219 at MOI=1, washed and fixed with
380 paraformaldehyde according to the 10x genomics cell preparation guide (CG000053) at various time
381 points (day 0, 1, 2, and 4) after infection. Single-cell suspensions (10^4 cells) were submitted to the
382 UC Davis Comprehensive Cancer Center (UCDCCC) Genomics Shared Resource for processing
383 on the Chromium Controller (10x Genomics) for cell partitioning into individual GEMs (gel bead-
384 in-emulsion), generation of barcoded cDNAs with unique molecular identifiers (UMIs), and
385 construction of barcoded sequencing libraries were constructed using the Chromium Single Cell
386 3' Reagent Kits v2 (10x Genomics). The libraries were then multiplexed and sequenced (~250
387 million mapped reads per sample) on an Illumina NovaSeq 6000 sequencing system. Single-cell
388 data were analyzed with the Cell Ranger v2.1 pipeline (10x Genomics). The pipeline included
389 alignment to the hg38 human reference genome and human herpesvirus 8 strain (GQ994935.1)
390 reference genome with STAR (Dobin et al., 2013), Uniform Manifold Approximation and Projection
391 (UMAP), and K-means clustering. Read count matrices obtained from the pipeline were
392 normalized using the log normalization method from the "Seurat" R package (Stuart et al., 2019).
393 We investigated the association between genes using the Pearson product-moment correlation
394 coefficient. To compute the correlation coefficient and p-value, we utilized the cor.test() function
395 from the stats package in R (R. Core Team, 2021).
396
397 **mRNA-seq.** RNA was prepared from infected monocytes using a QIAGEN RNeasy Miniprep kit
398 according to the manufacturer's protocol and submitted to the UCDCCC GSR for mRNA-seq

399 analysis. Indexed, stranded mRNA-seq libraries were prepared from total RNA (100 ng) using the
400 KAPA Stranded mRNA-Seq kit (Roche) according to the manufacturer's standard protocol.
401 Libraries were pooled and multiplex sequenced on an Illumina NovaSeq 6000 System (150-bp,
402 paired-end, >25 × 10^6 reads per sample). The RNA-Seq data was analyzed using a STAR-HTSeq-
403 DESeq2 pipeline. Raw sequence reads (FASTQ format) were mapped with STAR to the reference
404 human genome assembly (GRCh38/hg38, GENCODE release 36) and quantified with HTSeq
405 (Patro et al., 2017). The resulting data were first filtered by average normalized count data >1 and
406 volcano plots production and listing differentially expressed genes was performed by Subio
407 Platform ver. 1.24 (Subio Inc., Amami, Japan). For transcription factor analysis, differentially
408 expressed genes were submitted to Chip-Atlas to analyze common regulators and to predict
409 transcription factor binding (Oki et al., 2018).
410
411 **Phosphoflow PBMC CyTOF:** This assay was performed by the Human Immune Monitoring
412 Center at Stanford University. 2 x 10^6 PBMCs were infected with rKSHV.219, washed twice with
413 PBS and then fixed with paraformaldehyde. Cells were washed twice with CyFACS buffer (PBS
414 supplemented with 2% BSA, 2 mM EDTA, and 0.1% sodium azide) and stained for 30 min at
415 room temperature with 20 mL of surface antibody cocktail. Cells were washed twice with CyFACS,
416 permeabilized with 100% methanol, and kept at -80C overnight. The next day, cells were washed
417 with CyFACS buffer and resuspended in a 20 mL intracellular antibody cocktail in CyFACS for
418 30 min at room temperature before washing twice in CyFACS. Cells were resuspended in a 100
419 mL iridium-containing DNA intercalator (1:2000 dilution in 2% PFA in PBS) and incubated at
420 room temperature for 20 min. Cells were washed once with CyFACS buffer and twice with MilliQ
421 water. Cells were diluted to 750x10^5 cells/mL in MilliQ water and acquired on CyTOF. Data
422 analysis was performed using FlowJo v10.8.1 by gating on intact cells based on the iridium
423 isotopes from the intercalator, then on singlets by Ir191 vs cell length followed by cell subset-
424 specific gating as described in SFig. 2.

425 **Flow cytometry.** mAbs and isotype-matched controls were purchased from BD Bioscience
426 (BUV395 conjugated HLA-DR, BUV395 conjugated to CD11c, PerCP-Cy5.5 conjugated to
427 CD123, PE conjugated to CD11c, Alexa Fluor 647 conjugated to pSTAT-1, and Alexa Fluor 647
428 conjugated to pSTAT-3), and Biolegend (APC conjugated CD163, BV421 conjugated to CD16,
429 PE-Cy7 conjugated to Ki67, APC conjugated to PD-L1, APC conjugated to CD14, and Alexa

430 Fluor 488 conjugated to CD16). Cells in culture were washed twice with PBS and resuspended in
431 FACS buffer (PBS supplemented with 1% FBS) at $1x10^7$ cells/ml. 50 uL cells per well were
432 stained with Aqua LIVE/DEAD cell viability dye (Invitrogen, Carlsbad, CA) according to the
433 manufacturer's instructions, washed with FACS Buffer, and then stained for 45 min at room
434 temperature with antibodies. For intracellular staining of pSTAT1 and pSTAT3, cells were fixed
435 with paraformaldehyde, permeabilized with methanol, and kept at -80 C overnight. The cells were
436 washed with FACS buffer and stained with pSTAT-1 Alexa Fluor 647 and pSTAT-3 Alexa Fluor
437 647. Cells were washed three times with FACS buffer and resuspended in 200 uL FACS buffer.
438 For typical experiments, 10^5 PBMCs per sample were collected using DIVA 6.0 software on a
439 Fortessa flow cytometer (BD Biosciences) at the UCDCCC Flow Cytometry Shared Resource.
440 Data analysis was performed using FlowJo v10.8.1 by gating on live cells based on forward versus
441 side scatter profiles, then on singlets using forward scatter area versus height, followed by dead
442 cell exclusion using Aqua LIVE/DEAD viability dye, and then cell subset-specific gating.
443
444 **T cell proliferation assay.** Monocytes were infected with vIL6REV or vIL6STOP, or mock-infected
445 (PBS). Macrophages derived from KSHV-infected monocyte cultures were recovered at 7 dpi after being
446 washed with PBS twice followed by gentle pipetting and suspended in RPMI1640 medium containing
447 10% FBS. T cells were isolated from PBMCs using the EasySep™ Human CD3 positive selection kit II
448 (STEMCELL) according to the manufacturer's protocol. T cells were stained in PBS with the
449 CellTrace™ CFSE Cell Proliferation Kit (ThermoFisher) according to the manufacturer's protocol and
450 suspended in RPMI1640 medium containing 10% FBS. CSFE-labeled CD3+ T cells (10^4) were
451 incubated with 10^3 macrophages from KSHV-infected monocyte cultures in 200 uL/well in a 96-well U-
452 bottom plate, without or with 100 ng/ml anti-CD3 antibody (BD Bioscience) for 5 days. For positive and
453 negative controls, T cells were stimulated with ImmunoCult Human CD3/28 T cell activator (Stemcell)
454 or left unstimulated. Cells were recovered from cultures and analyzed using a BD Accuri™ flow
455 cytometer. Data analysis was performed using FlowJo v10.8.1 by gating lymphocytes based on
456 forward versus side scatter profiles. The average frequencies of the CFSE-negative population were
457 determined based on the negative control.
458
459 **Statistical analysis.** Statistical analyses were performed using GraphPad Prism 9.4.1 software.
460 Results are shown as mean ± SD with dots represent individual measurements. Statistical

461 significance was determined by Student's t-test, ratio paired t-test, or one-way ANOVA with Tukey's
462 multiple comparison test, and correction for false discovery rate (FDR) as described in each Figure
463 legend. FDR corrected $p < 0.05$ was considered statistically significant.
464
465
466 **Online supplemental material**
467 SFig.1 shows the characterization and validation of recombinant vIL6STOP and vIL6REV KSHV
468 and recombinant vIL6 used in this study. SFig.1A confirms the presence or absence of vIL6
469 expression in vIL6REV or vIL6STOP iSLK.219 cell lines that were used for virus preparation,
470 respectively, by Western blotting. SFig.1B shows the identity and purity of recombinant vIL6 and
471 its functionality to activate STAT1/3 in 293T and iSLK cell lines by Western blotting using a loss-
472 of-function vIL6 mutant as a control. SFig.2 illustrates the CyTOF phospho-panel markers and the
473 gating strategy used for analysis of immune cell subsets. SFig.3 shows GSEA analysis of RNAseq
474 data comparing vIL6REV-infected and uninfected macrophages with charts displaying the top 5
475 enriched upregulated and down regulated pathways.
476
477 **Data availability**
478 The scRNA-seq and RNA-seq data underlying Figs. 1 and 4 are openly available at GEO NCBI
479 under accession number GSE227167. The data underlying Fig.2 are available in
480 10.6084/m9.figshare.22273279). The data underlying Figs. 3 and 5 are available in the published
481 article and its online supplemental material. The reagents and cell lines are available upon
482 request from Y. Izumiya.
483
484 **Acknowledgment**
485 The authors would like to thank Dr. Robert Yarchoan (National Cancer Institute, USA) and Dr.
486 Harutaka Katano (National Institute of Infectious Disease, Japan) for the generous gift of rabbit
487 antibodies against vIL6. We would like to thank Andreas Koni for his assistance in preparing the
488 manuscript. We would like to thank Immune Modeling, Analysis and Diagnostic, Genomics, and
489 Flow Cytometry Shared Resources of the UC Davis Comprehensive Cancer Center Shared
490 Resources for expert support with 10x Genomics scRNA-seq, total RNA-seq, and flow

cytometry analyses, and the Stanford Human Immune Monitoring Center for expert CyTOF analysis.

M.S. and Y.I. are founders of VGN BIO, Inc. The authors have no additional financial interests.

This work was supported by grants from the National Cancer Institute CA232845-02S1 (M. Shimoda), CA225266, CA232845, and AI167663 (Y. Izumiya), and UC Davis Dermatology Seed grant (M. Shimoda). M. Shimoda was supported by the National Cancer Institute/CRCHD/CURE program. The Immune Modeling, Analysis and Diagnostic, Genomics, and Flow Cytometry Shared Resources are supported by the UC Davis Comprehensive Cancer Center Support Grant (CCSG) awarded by the National Cancer Institute (NCI P30CA093373).

Author contributions

Conceptualization: M. Shimoda, and Y. Izumiya. Experimental design: M. Shimoda and Y. Izumiya. Experiment and Data acquisition and analysis: M. Shimoda, R. Davis, A. Merleev, T. Inagaki, and Y. Izumiya. Funding acquisition: M. Shimoda and Y. Izumiya. Manuscript preparation: M. Shimoda. Review & Editing: M. Shimoda, R. Davis, A. Merleev, C.G. Tepper, E. Maverakis, T. Inagaki, and Y. Izumiya.

511 **Figure 1. KSHV preferentially infects monocytes and triggers the monocyte inflammatory**
512 **transcription program**. PBMCs were infected with rKSHV.219 at MOI=1, fixed at various time
513 points (pre-infection, day 1, 2, and 4) after infection, and subjected to 10x Genomics Chromium scRNA-
514 seq analysis. (A) UMAP visualizes 9 PBMC clusters in a preinfectional sample based on lineage-specific
515 gene expression of *KLRD1, CD14, APOBEC3A, VMO1, CD79A*, and *CD3E* genes for NK cells,
516 monocytes, intermediate monocytes, non-classical monocytes, B cells, and T cells, respectively. (B)
517 KSHV-encoded K2 (vIL6) expression overlapped with CD14 expression at 1 dpi. (C) The kinetic
518 scRNA-seq analysis on pre-infection, 1 dpi, 2 dpi, and 4 dpi revealed that KSHV infection in $CD14^+$
519 monocytes triggered the activation and inflammatory response with the upregulation of *IL3RA* (CD123),
520 *CCL2*, and *TNFα*. (D) Expression of genes in $CD14^+$ monocytes associated with differentiation of M2-
521 like macrophages with suppressive phenotype (*CD274/PD-L1*, *C1QA*, *RNASE1*, *IL-10*, and *CD163*).
522 Gene expression levels are indicated by heatmap bars. A representative of three similar experiments is
523 shown.
524
525 **Figure 2. KSHV infection preferentially triggers STAT activation in monocytes and**
526 **dendritic cells**. PBMC from healthy donors (n=6) were infected with vIL6REV (KSHV with vIL6
527 expression) or vIL6STOP (KSHV without vIL6 expression) (MOI=1), or mock-infected (PBS). At 1
528 dpi, cells were fixed and subjected to CyTOF analysis. The expression levels of 10 signaling molecules
529 were evaluated. Data combine two experiments (n=3 each). (A) tSNE for dimension reduction analysis
530 was applied for each infection group after 1000 events from 6 samples in each group were
531 concatenated. Immune cell subsets were clustered based on each lineage's marker expression (Right
532 panel). (B) The phenotypic changes induced in three immune cell populations corresponding to
533 $CD4^+CD3^+$, $CD19^+CD20^-$, and $CD123^+CD14^+$ clusters by infection were identified by comparison
534 between vIL6STOP, vIL-6REV, and the mock-infected (PBS) control group. (C) The activation status
535 of 10 signaling molecules among plasmacytoid dendritic cells (pDC) and monocytic cell subsets
536 including $CD123^+CD11c^+$ cells, myeloid (m)DC, $CD14^{lo}CD16^+$ non-classical monocytes,
537 $CD14^+CD16^+$ intermediate monocytes, and $CD14^-CD16^+$ classical monocytes are shown in heat maps.
538 Each subset was identified based on the lineage cell surface marker expression with gating strategies
539 shown in SFig.2. (D) The fold change in the CyTOF signal intensity of STAT1 and pSTAT3 for
540 $CD123^+CD11c^+$ cells (TOP panel) and $CD14^+CD16^+$ cells (Bottom panel) in infected groups compared
541 to mock-infected (PBS) control group are shown. p values shown are by ratio paired t-test. $p<0.05$:

542 statistically significant. (E) Individual percentages of pDCs, $CD14^+CD16^+$, and $CD123^+CD11c^+$ cells
543 among DC gate for each PBMC sample (n=6) are compared between vIL6REV- and vIL6STOP-
544 infected groups, and the uninfected group (PBS). p values shown are by ratio paired t-test. $p<0.05$:
545 statistically significant.
546
547 **Figure 3. KSHV preferentially infects and expands CD14+ monocytes with an inflammatory**
548 **response in a manner dependent on vIL6**. Monocytes were isolated negatively from PBMCs (n=6)
549 using magnetic beads-based negative enrichment and infected with vIL6STOP or vIL6REV rKSHV
550 (MOI=1). (A) The frequencies of live cells at 2 dpi by live/dead staining are shown (B) Representative
551 FACS profiles of infected monocytes analyzed by flow cytometry for Ki67, CD16, and PD-L1
552 expressing cells. (C) The frequencies for Ki67+, CD16+, and PDL-1+ cells are shown. Data represent
553 two similar experiments. (D) Representative images of cell blasts in the indicated treatment conditions
554 (x100). (E) Representative FACS profiles of each sample for pSTAT1 and pSTAT3 intracellular
555 staining with the percentage of gated pSTAT1- and pSTAT3- expressing cells are shown. Data
556 represent two similar experiments. *p* values shown are by ANOVA with a paired comparison with
557 Tukey's multiple comparison test. $p < 0.05$: statistically significant.
558
559 **Figure 4. Differential gene expression analysis between wild-type KSHV and vIL6 deficient**
560 **KSHV infected monocytes**. (A) A schematic illustration of the KSHV infection experiment
561 (Left). Monocytes were infected with vIL6REV, vIL6STOP, or mock-infected (PBS). At 7 dpi,
562 cells were harvested for RNA-seq analysis (n=2/group). Principal component analysis (PCA) of
563 RNA-seq data from independent biological replicates is shown (Right). The number in
564 parenthesis indicates the percentage of total variance explained by each PC. Colored dots
565 represent individual samples infected with mock (PBS-treated), vIL6REV, and vIL6STOP. (B)
566 Volcano plots for differentially expressed genes (log2 FC threshold = 1, *p*-value threshold =
567 0.05) between vIL6REV and vIL6STOP (Top), vIL6 REV and mock (Middle) and vIL6STOP
568 and mock (Bottom). The log2 FC indicates the mean expression for each. The functional
569 enrichment analysis of upregulated genes (C) and downregulated genes (D) in vIL6REV-
570 compared to vIL6STOP-infected monocytes. DAVID functional enrichment analysis was
571 performed, and the analysis results of the top 5 enriched pathways are shown (Right). The
572 representative results of Gene Set Enrichment Analysis (GSEA) are shown (Left). (E) Heatmap

573 of representative genes from enriched gene sets for upregulated IFN-inducible genes (C) or
574 downregulated MHC-II genes (D) in vIL6REV- compared to vIL6STOP-infected monocytes. (F)
575 Putative transcription factors that are responsible for differentially expressed genes between vIL-
576 6 REV and vIL-6 STOP KSHV infection. The bar charts indicate *p* values for enrichment. The
577 following parameters were used; Organism: Homo sapiens (hg38), Experiment type: ChiP (TFs
578 and others), Cell type Class: Blood, and Threshold for significance: 50.
579
580 **Figure 5. KSHV infection promotes macrophage differentiation with an immunosuppressive**
581 **phenotype in a manner dependent on vIL6 expression**. Monocytes were infected with vIL6REV or
582 vIL6STOP (MOI=1), uninfected (PBS) and cultured for 7-14 days, or treated with vIL6 (200 ng/ml in
583 serum-free medium) for 9 days. Each sample was analyzed by flow cytometry with isotype control
584 staining as a control. (A) The average frequency of macrophages in each culture (n=3) is based on
585 representative FSC-H and SSC-H profiles. Data combine four independent experiments with different
586 donor samples. Dots represent the average % of biological replicates (n=2-3). (B) The average geometric
587 mean fluorescent intensity (gMFI) of HLA-DR for each macrophage sample with representative overlays
588 are shown. Data combine four independent experiments with different donor samples. Dots represent the
589 average HLA-DR gMFI of biological replicates (n=2-3). (C) Representative FACS plots of live
590 monocytes one week after vIL6 treatment and the average frequencies (n=3) are shown. (D) The average
591 gMFI of HLA-DR for each macrophage sample in (C) with representative overlays are shown. Data
592 represent two similar experiments. (E) An experimental design of T cell proliferation assay with
593 macrophages (Top) and representative histograms of T cells (gated based on FSC-A and SSC-A) for
594 CSFE are shown. T cells without or with anti-CD3/CD28 tetramer stimulation are used as controls. (F)
595 The average frequencies of the CFSE-negative population determined as in (E) for each sample are
596 shown (n=3). *p* values shown are by ANOVA with a paired comparison with Tukey's multiple
597 comparison test. $p < 0.05$: statistically significant. Data represent two similar experiments.
598
599

600 **References**

601 Alomari, N., and J. Totonchy. 2020. Cytokine-Targeted Therapeutics for KSHV-Associated
602 Disease. *Viruses* 12:
603 Aoki, Y., R. Yarchoan, K. Wyvill, S. Okamoto, R.F. Little, and G. Tosato. 2001. Detection of
604 viral interleukin-6 in Kaposi sarcoma-associated herpesvirus-linked disorders. *Blood*
605 97:2173-2176.
606 Baasch, S., P. Giansanti, J. Kolter, A. Riedl, A.J. Forde, S. Runge, S. Zenke, R. Elling, A.
607 Halenius, S. Brabletz, H. Hengel, B. Kuster, T. Brabletz, L. Cicin-Sain, R. Arens, A.
608 Vlachos, J.C. Rohr, M.P. Stemmler, M. Kopf, Z. Ruzsics, and P. Henneke. 2021.
609 Cytomegalovirus subverts macrophage identity. *Cell* 184:3774-3793 e3725.
610 Baasch, S., Z. Ruzsics, and P. Henneke. 2020. Cytomegaloviruses and Macrophages-Friends and
611 Foes From Early on? *Front Immunol* 11:793.
612 Bhaskaran, N., S.K. Ghosh, X. Yu, S. Qin, A. Weinberg, P. Pandiyan, and F. Ye. 2017. Kaposi's
613 sarcoma-associated herpesvirus infection promotes differentiation and polarization of
614 monocytes into tumor-associated macrophages. *Cell Cycle* 16:1611-1621.
615 Campbell, D.M., G. Rappocciolo, F.J. Jenkins, and C.R. Rinaldo. 2014. Dendritic cells: key
616 players in human herpesvirus 8 infection and pathogenesis. *Front Microbiol* 5:452.
617 Caro-Vegas, C., S. Sellers, K.M. Host, J. Seltzer, J. Landis, W.A. Fischer, 2nd, B. Damania, and
618 D.P. Dittmer. 2020. Runaway Kaposi Sarcoma-associated herpesvirus replication
619 correlates with systemic IL-10 levels. *Virology* 539:18-25.
620 Cesarman, E., B. Damania, S.E. Krown, J. Martin, M. Bower, and D. Whitby. 2019. Kaposi
621 sarcoma. *Nat Rev Dis Primers* 5:9.
622 Chandriani, S., and D. Ganem. 2010. Array-based transcript profiling and limiting-dilution
623 reverse transcription-PCR analysis identify additional latent genes in Kaposi's sarcoma-
624 associated herpesvirus. *J Virol* 84:5565-5573.
625 Cojohari, O., J. Mahmud, A.M. Altman, M.A. Peppenelli, M.J. Miller, and G.C. Chan. 2020.
626 Human Cytomegalovirus Mediates Unique Monocyte-to-Macrophage Differentiation
627 through the PI3K/SHIP1/Akt Signaling Network. *Viruses* 12:
628 Decker, L.L., P. Shankar, G. Khan, R.B. Freeman, B.J. Dezube, J. Lieberman, and D.A. Thorley-
629 Lawson. 1996. The Kaposi sarcoma-associated herpesvirus (KSHV) is present as an
630 intact latent genome in KS tissue but replicates in the peripheral blood mononuclear cells
631 of KS patients. *J Exp Med* 184:283-288.
632 Dittmer, D.P., and B. Damania. 2019. Kaposi's Sarcoma-Associated Herpesvirus (KSHV)-
633 Associated Disease in the AIDS Patient: An Update. *Cancer Treat Res* 177:63-80.
634 Dobin, A., C.A. Davis, F. Schlesinger, J. Drenkow, C. Zaleski, S. Jha, P. Batut, M. Chaisson, and
635 T.R. Gingeras. 2013. STAR: ultrafast universal RNA-seq aligner. *Bioinformatics* 29:15-
636 21.
637 Dumic, I., M. Radovanovic, O. Igandan, I. Savic, C.W. Nordstrom, D. Jevtic, A. Subramanian,
638 and P. Ramanan. 2020. A Fatal Case of Kaposi Sarcoma Immune Reconstitution
639 Syndrome (KS-IRIS) Complicated by Kaposi Sarcoma Inflammatory Cytokine Syndrome
640 (KICS) or Multicentric Castleman Disease (MCD): A Case Report and Review. *Am J*
641 *Case Rep* 21:e926433.
642 Fullwood, R.A., G.M. Low, E.P. Chase, M. Grasley, S.S. Beal, I.M. McCrary, C.W. Daniels, K.
643 Ingersoll, and B.K. Berges. 2018. The Kaposi's sarcoma-associated herpesvirus viral
644 interleukin 6 gene affects metastasis and expression of B cell markers in a murine
645 xenograft model. *PLoS One* 13:e0204947.

646 Gane, J.M., R.A. Stockley, and E. Sapey. 2016. TNF-alpha Autocrine Feedback Loops in Human
647 Monocytes: The Pro- and Anti-Inflammatory Roles of the TNF-alpha Receptors Support
648 the Concept of Selective TNFR1 Blockade In Vivo. *J Immunol Res* 2016:1079851.
649 Giffin, L., J.A. West, and B. Damania. 2015. Kaposi's Sarcoma-Associated Herpesvirus
650 Interleukin-6 Modulates Endothelial Cell Movement by Upregulating Cellular Genes
651 Involved in Migration. *mBio* 6:e01499-01415.
652 Gilardini Montani, M.S., L. Falcinelli, R. Santarelli, M. Granato, M.A. Romeo, N. Cecere, R.
653 Gonnella, G. D'Orazi, A. Faggioni, and M. Cirone. 2020. KSHV infection skews
654 macrophage polarisation towards M2-like/TAM and activates Ire1 alpha-XBP1 axis up-
655 regulating pro-tumorigenic cytokine release and PD-L1 expression. *Br J Cancer* 123:298-
656 306.
657 Goncalves, P.H., J. Ziegelbauer, T.S. Uldrick, and R. Yarchoan. 2017. Kaposi sarcoma
658 herpesvirus-associated cancers and related diseases. *Curr Opin HIV AIDS* 12:47-56.
659 Gregory, S.M., L. Wang, J.A. West, D.P. Dittmer, and B. Damania. 2012. Latent Kaposi's
660 sarcoma-associated herpesvirus infection of monocytes downregulates expression of
661 adaptive immune response costimulatory receptors and proinflammatory cytokines. *J*
662 *Virol* 86:3916-3923.
663 Hijdra, D., A.D. Vorselaars, J.C. Grutters, A.M. Claessen, and G.T. Rijkers. 2012. Differential
664 expression of TNFR1 (CD120a) and TNFR2 (CD120b) on subpopulations of human
665 monocytes. *J Inflamm (Lond)* 9:38.
666 Hoenen, T., and A. Groseth. 2022. Virus-Host Cell Interactions. *Cells* 11:
667 Kapellos, T.S., L. Bonaguro, I. Gemund, N. Reusch, A. Saglam, E.R. Hinkley, and J.L. Schultze.
668 2019. Human Monocyte Subsets and Phenotypes in Major Chronic Inflammatory
669 Diseases. *Front Immunol* 10:2035.
670 McNab, F., K. Mayer-Barber, A. Sher, A. Wack, and A. O'Garra. 2015. Type I interferons in
671 infectious disease. *Nat Rev Immunol* 15:87-103.
672 McNab, F.W., J. Ewbank, A. Howes, L. Moreira-Teixeira, A. Martirosyan, N. Ghilardi, M.
673 Saraiva, and A. O'Garra. 2014. Type I IFN induces IL-10 production in an IL-27-
674 independent manner and blocks responsiveness to IFN-gamma for production of IL-12
675 and bacterial killing in Mycobacterium tuberculosis-infected macrophages. *J Immunol*
676 193:3600-3612.
677 Molden, J., Y. Chang, Y. You, P.S. Moore, and M.A. Goldsmith. 1997. A Kaposi's sarcoma-
678 associated herpesvirus-encoded cytokine homolog (vIL-6) activates signaling through the
679 shared gp130 receptor subunit. *J Biol Chem* 272:19625-19631.
680 Morris, V.A., A.S. Punjabi, and M. Lagunoff. 2008. Activation of Akt through gp130 receptor
681 signaling is required for Kaposi's sarcoma-associated herpesvirus-induced lymphatic
682 reprogramming of endothelial cells. *J Virol* 82:8771-8779.
683 Morris, V.A., A.S. Punjabi, R.C. Wells, C.J. Wittkopp, R. Vart, and M. Lagunoff. 2012. The
684 KSHV viral IL-6 homolog is sufficient to induce blood to lymphatic endothelial cell
685 differentiation. *Virology* 428:112-120.
686 Oki, S., T. Ohta, G. Shioi, H. Hatanaka, O. Ogasawara, Y. Okuda, H. Kawaji, R. Nakaki, J. Sese,
687 and C. Meno. 2018. ChIP-Atlas: a data-mining suite powered by full integration of public
688 ChIP-seq data. *EMBO Rep* 19:
689 Olson, G.S., T.A. Murray, A.N. Jahn, D. Mai, A.H. Diercks, E.S. Gold, and A. Aderem. 2021.
690 Type I interferon decreases macrophage energy metabolism during mycobacterial
691 infection. *Cell Rep* 35:109195.

692 Patro, R., G. Duggal, M.I. Love, R.A. Irizarry, and C. Kingsford. 2017. Salmon provides fast and
693 bias-aware quantification of transcript expression. *Nat Methods* 14:417-419.
694 Polizzotto, M.N., T.S. Uldrick, D. Hu, and R. Yarchoan. 2012. Clinical Manifestations of Kaposi
695 Sarcoma Herpesvirus Lytic Activation: Multicentric Castleman Disease (KSHV-MCD)
696 and the KSHV Inflammatory Cytokine Syndrome. *Front Microbiol* 3:73.
697 Polizzotto, M.N., T.S. Uldrick, K.M. Wyvill, K. Aleman, V. Marshall, V. Wang, D. Whitby, S.
698 Pittaluga, E.S. Jaffe, C. Millo, G. Tosato, R.F. Little, S.M. Steinberg, I. Sereti, and R.
699 Yarchoan. 2016. Clinical Features and Outcomes of Patients With Symptomatic Kaposi
700 Sarcoma Herpesvirus (KSHV)-associated Inflammation: Prospective Characterization of
701 KSHV Inflammatory Cytokine Syndrome (KICS). *Clin Infect Dis* 62:730-738.
702 Qin, Z., P. Kearney, K. Plaisance, and C.H. Parsons. 2010. Pivotal advance: Kaposi's sarcoma-
703 associated herpesvirus (KSHV)-encoded microRNA specifically induce IL-6 and IL-10
704 secretion by macrophages and monocytes. *J Leukoc Biol* 87:25-34.
705 Rappocciolo, G., F.J. Jenkins, H.R. Hensler, P. Piazza, M. Jais, L. Borowski, S.C. Watkins, and
706 C.R. Rinaldo, Jr. 2006. DC-SIGN is a receptor for human herpesvirus 8 on dendritic cells
707 and macrophages. *J Immunol* 176:1741-1749.
708 Redpath, S., A. Angulo, N.R. Gascoigne, and P. Ghazal. 1999. Murine cytomegalovirus infection
709 down-regulates MHC class II expression on macrophages by induction of IL-10. *J*
710 *Immunol* 162:6701-6707.
711 Sakakibara, S., and G. Tosato. 2011. Viral interleukin-6: role in Kaposi's sarcoma-associated
712 herpesvirus: associated malignancies. *J Interferon Cytokine Res* 31:791-801.
713 Shnayder, M., A. Nachshon, B. Rozman, B. Bernshtein, M. Lavi, N. Fein, E. Poole, S. Avdic, E.
714 Blyth, D. Gottlieb, A. Abendroth, B. Slobedman, J. Sinclair, N. Stern-Ginossar, and M.
715 Schwartz. 2020. Single cell analysis reveals human cytomegalovirus drives latently
716 infected cells towards an anergic-like monocyte state. *Elife* 9:
717 Staskus, K.A., W. Zhong, K. Gebhard, B. Herndier, H. Wang, R. Renne, J. Beneke, J. Pudney,
718 D.J. Anderson, D. Ganem, and A.T. Haase. 1997. Kaposi's sarcoma-associated
719 herpesvirus gene expression in endothelial (spindle) tumor cells. *J Virol* 71:715-719.
720 Suthaus, J., C. Stuhlmann-Laeisz, V.S. Tompkins, T.R. Rosean, W. Klapper, G. Tosato, S. Janz,
721 J. Scheller, and S. Rose-John. 2012. HHV-8-encoded viral IL-6 collaborates with mouse
722 IL-6 in the development of multicentric Castleman disease in mice. *Blood* 119:5173-
723 5181.
724 Uccini, S., M.C. Sirianni, L. Vincenzi, S. Topino, A. Stoppacciaro, I. Lesnoni La Parola, M.
725 Capuano, C. Masini, D. Cerimele, M. Cella, A. Lanzavecchia, P. Allavena, A.
726 Mantovani, C.D. Baroni, and L.P. Ruco. 1997. Kaposi's sarcoma cells express the
727 macrophage-associated antigen mannose receptor and develop in peripheral blood
728 cultures of Kaposi's sarcoma patients. *Am J Pathol* 150:929-938.
729 Uhlen, M., M.J. Karlsson, W. Zhong, A. Tebani, C. Pou, J. Mikes, T. Lakshmikanth, B.
730 Forsstrom, F. Edfors, J. Odeberg, A. Mardinoglu, C. Zhang, K. von Feilitzen, J. Mulder,
731 E. Sjostedt, A. Hober, P. Oksvold, M. Zwahlen, F. Ponten, C. Lindskog, A. Sivertsson, L.
732 Fagerberg, and P. Brodin. 2019. A genome-wide transcriptomic analysis of protein-
733 coding genes in human blood cells. *Science* 366:
734 van der Meulen, E., M. Anderton, M.J. Blumenthal, and G. Schafer. 2021. Cellular Receptors
735 Involved in KSHV Infection. *Viruses* 13:
736 Watanabe, S., M. Alexander, A.V. Misharin, and G.R.S. Budinger. 2019. The role of
737 macrophages in the resolution of inflammation. *J Clin Invest* 129:2619-2628.

738 Webster, J.D., and D. Vucic. 2020. The Balance of TNF Mediated Pathways Regulates
739 Inflammatory Cell Death Signaling in Healthy and Diseased Tissues. *Front Cell Dev Biol*
740 8:365.
741 Wolf, Y., A. Shemer, M. Polonsky, M. Gross, A. Mildner, S. Yona, E. David, K.W. Kim, T.
742 Goldmann, I. Amit, M. Heikenwalder, S. Nedospasov, M. Prinz, N. Friedman, and S.
743 Jung. 2017. Autonomous TNF is critical for in vivo monocyte survival in steady state and
744 inflammation. *J Exp Med* 214:905-917.
745 Yeap, W.H., K.L. Wong, N. Shimasaki, E.C. Teo, J.K. Quek, H.X. Yong, C.P. Diong, A.
746 Bertoletti, Y.C. Linn, and S.C. Wong. 2016. CD16 is indispensable for antibody-
747 dependent cellular cytotoxicity by human monocytes. *Sci Rep* 6:34310.
748 Zdrenghea, M.T., H. Makrinioti, A. Muresan, S.L. Johnston, and L.A. Stanciu. 2015. The role of
749 macrophage IL-10/innate IFN interplay during virus-induced asthma. *Rev Med Virol*
750 25:33-49.
751 Zhang, L., X. Jiang, D. Pfau, Y. Ling, and C.F. Nathan. 2021. Type I interferon signaling
752 mediates Mycobacterium tuberculosis-induced macrophage death. *J Exp Med* 218:
753 Zhu, X., Y. Guo, S. Yao, Q. Yan, M. Xue, T. Hao, F. Zhou, J. Zhu, D. Qin, and C. Lu. 2014.
754 Synergy between Kaposi's sarcoma-associated herpesvirus (KSHV) vIL-6 and HIV-1 Nef
755 protein in promotion of angiogenesis and oncogenesis: role of the AKT signaling
756 pathway. *Oncogene* 33:1986-1996.
757

758

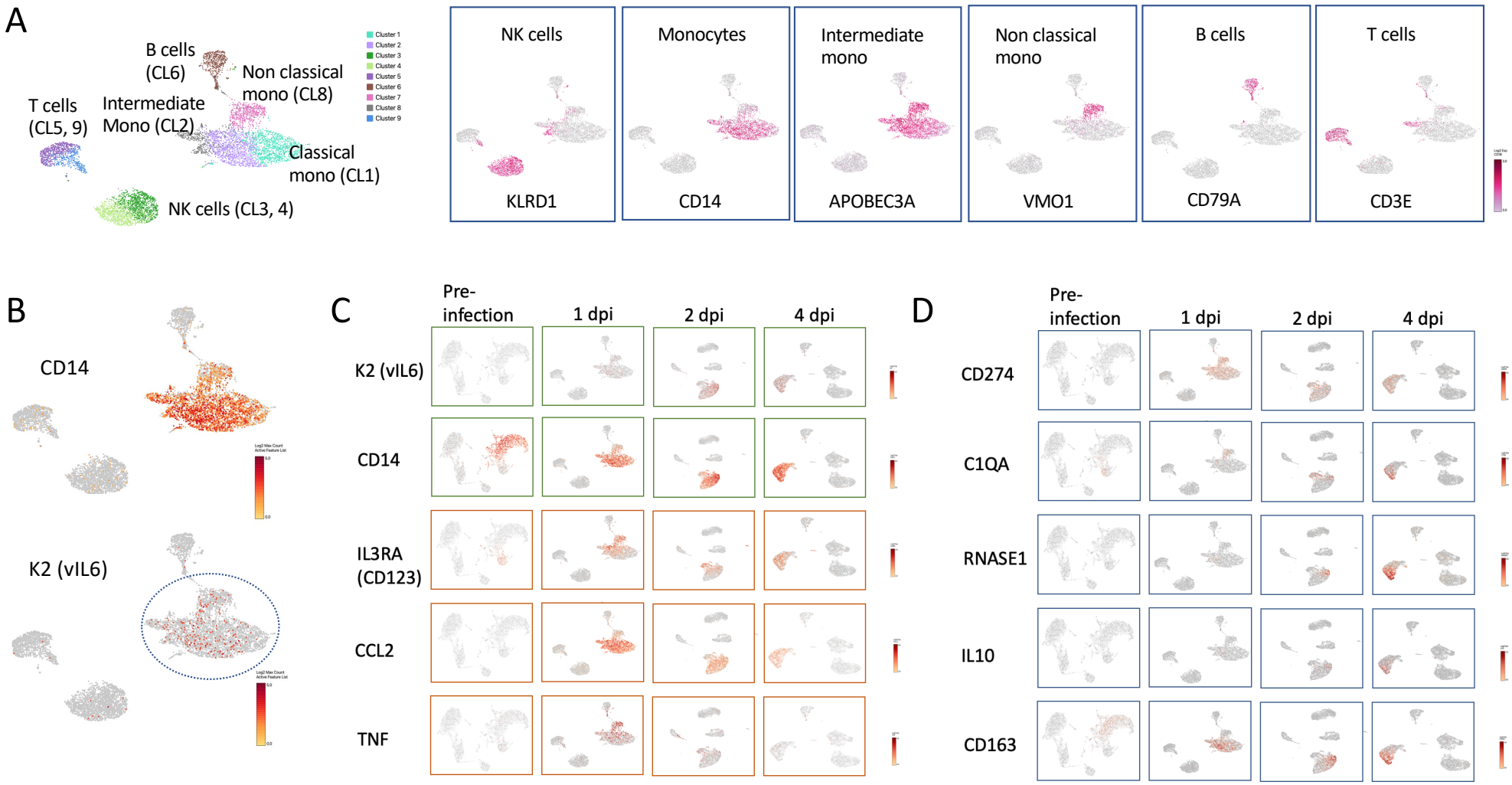
A
B cells (CL6)
Non classical mono (CL8)
T cells (CL5, 9)
Intermediate Mono (CL2)
Classical mono (CL1)
NK cells (CL3, 4)
Cluster 1
Cluster 2
Cluster 3
Cluster 4
Cluster 5
Cluster 6
Cluster 7
Cluster 8
Cluster 9
NK cells
KLRD1
Monocytes
CD14
Intermediate mono
APOBEC3A
Non classical mono
VMO1
B cells
CD79A
T cells
CD3E
B
CD14
K2 (vIL6)
C
Pre-infection
1 dpi
2 dpi
4 dpi
K2 (vIL6)
CD14
IL3RA (CD123)
CCL2
TNF
D
Pre-infection
1 dpi
2 dpi
4 dpi
CD274
C1QA
RNASE1
IL10
CD163

Figure 1

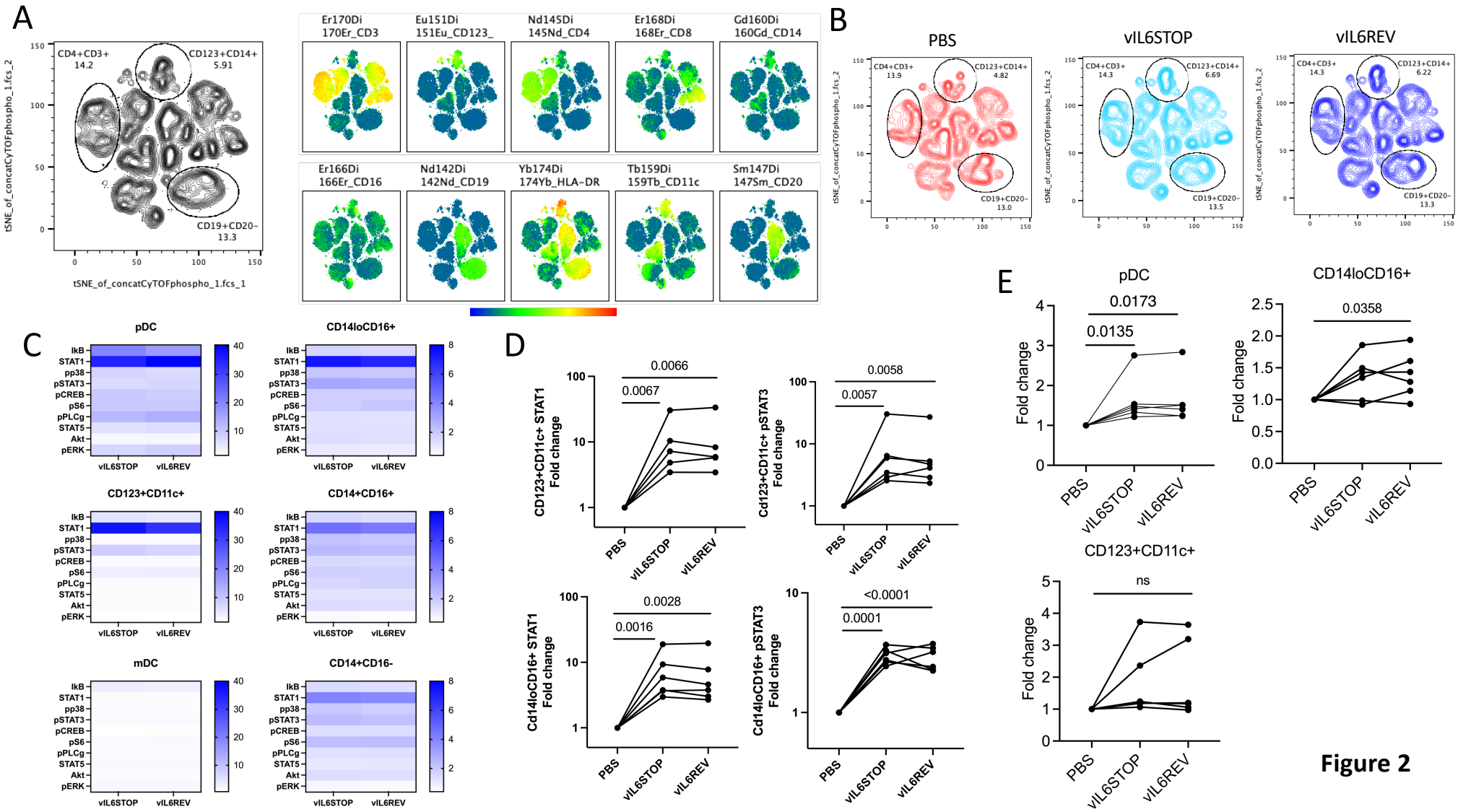
A
CD4+CD3+ 14.2
CD123+CD14+ 5.91
CD19+CD20- 13.3
tSNE_of_concatCyTOFphospho_1.fcs_1
tSNE_of_concatCyTOFphospho_1.fcs_2
Er170Di 170Er_CD3
Eu151Di 151Eu_CD123_
Nd145Di 145Nd_CD4
Er168Di 168Er_CD8
Gd160Di 160Gd_CD14
Er166Di 166Er_CD16
Nd142Di 142Nd_CD19
Yb174Di 174Yb_HLA-DR
Tb159Di 159Tb_CD11c
Sm147Di 147Sm_CD20
B
PBS
vIL6STOP
vIL6REV
CD4+CD3+ 13.9
CD123+CD14+ 4.82
CD19+CD20- 13.0
CD4+CD3+ 14.3
CD123+CD14+ 6.69
CD19+CD20- 13.5
CD4+CD3+ 14.3
CD123+CD14+ 6.22
CD19+CD20- 13.3
C
pDC
CD14loCD16+
CD123+CD11c+
CD14+CD16+
mDC
CD14+CD16-
IkB
STAT1
pp38
pSTAT3
pCREB
pS6
pPLCg
STAT5
Akt
pERK
vIL6STOP
vIL6REV
D
CD123+CD11c+ STAT1 Fold change
0.0066
0.0067
Cd123+CD11c+ pSTAT3 Fold change
0.0058
0.0057
Cd14loCD16+ STAT1 Fold change
0.0028
0.0016
Cd14loCD16+ pSTAT3 Fold change
<0.0001
0.0001
PBS
vIL6STOP
vIL6REV
E
pDC
0.0173
0.0135
CD14loCD16+
0.0358
CD123+CD11c+
ns
Fold change
PBS
vIL6STOP
vIL6REV

Figure 2

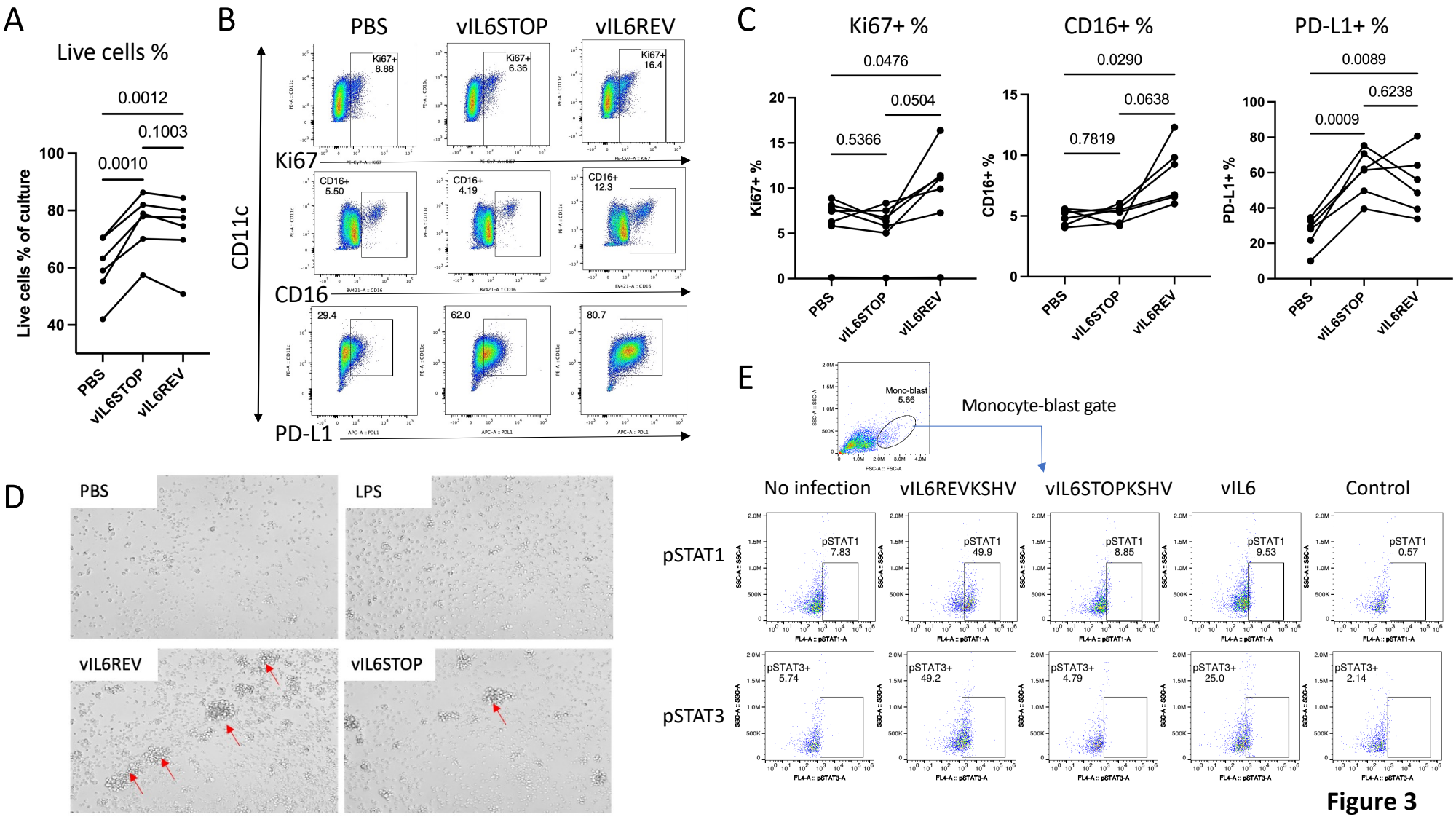
A
Live cells %
0.0012
0.1003
0.0010
Live cells % of culture
100
80
60
40
PBS
vIL6STOP
vIL6REV
B
PBS
vIL6STOP
vIL6REV
CD11c
Ki67
CD16
PD-L1
Ki67+ 8.88
Ki67+ 6.36
Ki67+ 16.4
CD16+ 5.50
CD16+ 4.19
CD16+ 12.3
29.4
62.0
80.7
C
Ki67+ %
CD16+ %
PD-L1+ %
0.0476
0.0504
0.5366
0.0290
0.0638
0.7819
0.0089
0.6238
0.0009
D
PBS
LPS
vIL6REV
vIL6STOP
E
Mono-blast 5.66
Monocyte-blast gate
No infection
vIL6REVKSHV
vIL6STOPKSHV
vIL6
Control
pSTAT1
pSTAT3
pSTAT1 7.83
pSTAT1 49.9
pSTAT1 8.85
pSTAT1 9.53
pSTAT1 0.57
pSTAT3+ 5.74
pSTAT3+ 49.2
pSTAT3+ 4.79
pSTAT3+ 25.0
pSTAT3+ 2.14

Figure 3

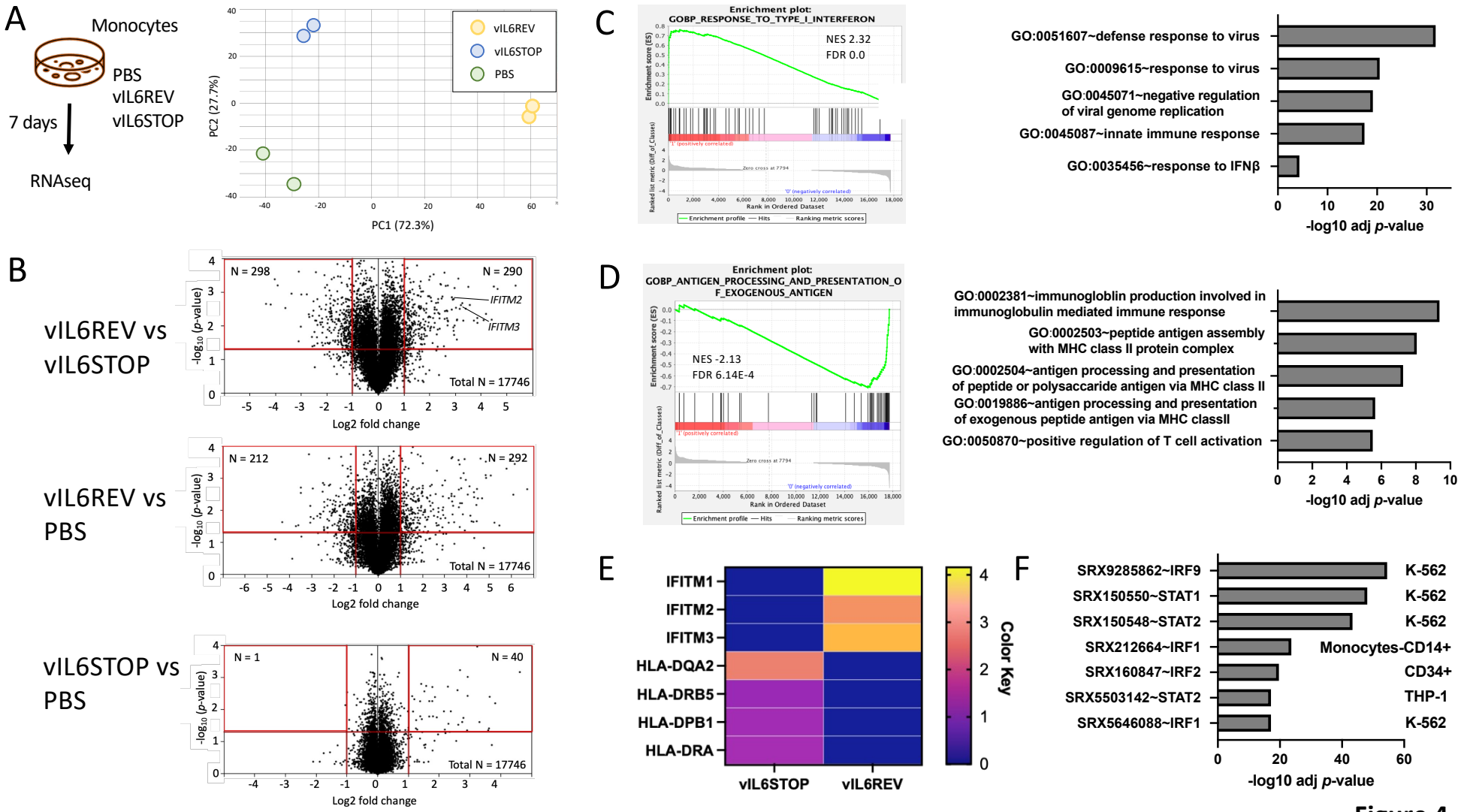
A
Monocytes
PBS
vIL6REV
vIL6STOP
7 days
RNAseq
vIL6REV
vIL6STOP
PBS
PC2 (27.7%)
PC1 (72.3%)
B
vIL6REV vs vIL6STOP
N = 298
N = 290
IFITM2
IFITM3
Total N = 17746
Log2 fold change
vIL6REV vs PBS
N = 212
N = 292
Total N = 17746
Log2 fold change
vIL6STOP vs PBS
N = 1
N = 40
Total N = 17746
Log2 fold change
C
Enrichment plot:
GOBP_RESPONSE_TO_TYPE_I_INTERFERON
NES 2.32
FDR 0.0
GO:0051607~defense response to virus
GO:0009615~response to virus
GO:0045071~negative regulation of viral genome replication
GO:0045087~innate immune response
GO:0035456~response to IFNβ
-log10 adj p-value
D
Enrichment plot:
GOBP_ANTIGEN_PROCESSING_AND_PRESENTATION_OF_EXOGENOUS_ANTIGEN
NES -2.13
FDR 6.14E-4
GO:0002381~immunogloblin production involved in immunoglobulin mediated immune response
GO:0002503~peptide antigen assembly with MHC class II protein complex
GO:0002504~antigen processing and presentation of peptide or polysaccaride antigen via MHC class II
GO:0019886~antigen processing and presentation of exogenous peptide antigen via MHC classII
GO:0050870~positive regulation of T cell activation
-log10 adj p-value
E
IFITM1
IFITM2
IFITM3
HLA-DQA2
HLA-DRB5
HLA-DPB1
HLA-DRA
vIL6STOP
vIL6REV
Color Key
F
SRX9285862~IRF9
SRX150550~STAT1
SRX150548~STAT2
SRX212664~IRF1
SRX160847~IRF2
SRX5503142~STAT2
SRX5646088~IRF1
K-562
K-562
K-562
Monocytes-CD14+
CD34+
THP-1
K-562
-log10 adj p-value

Figure 4

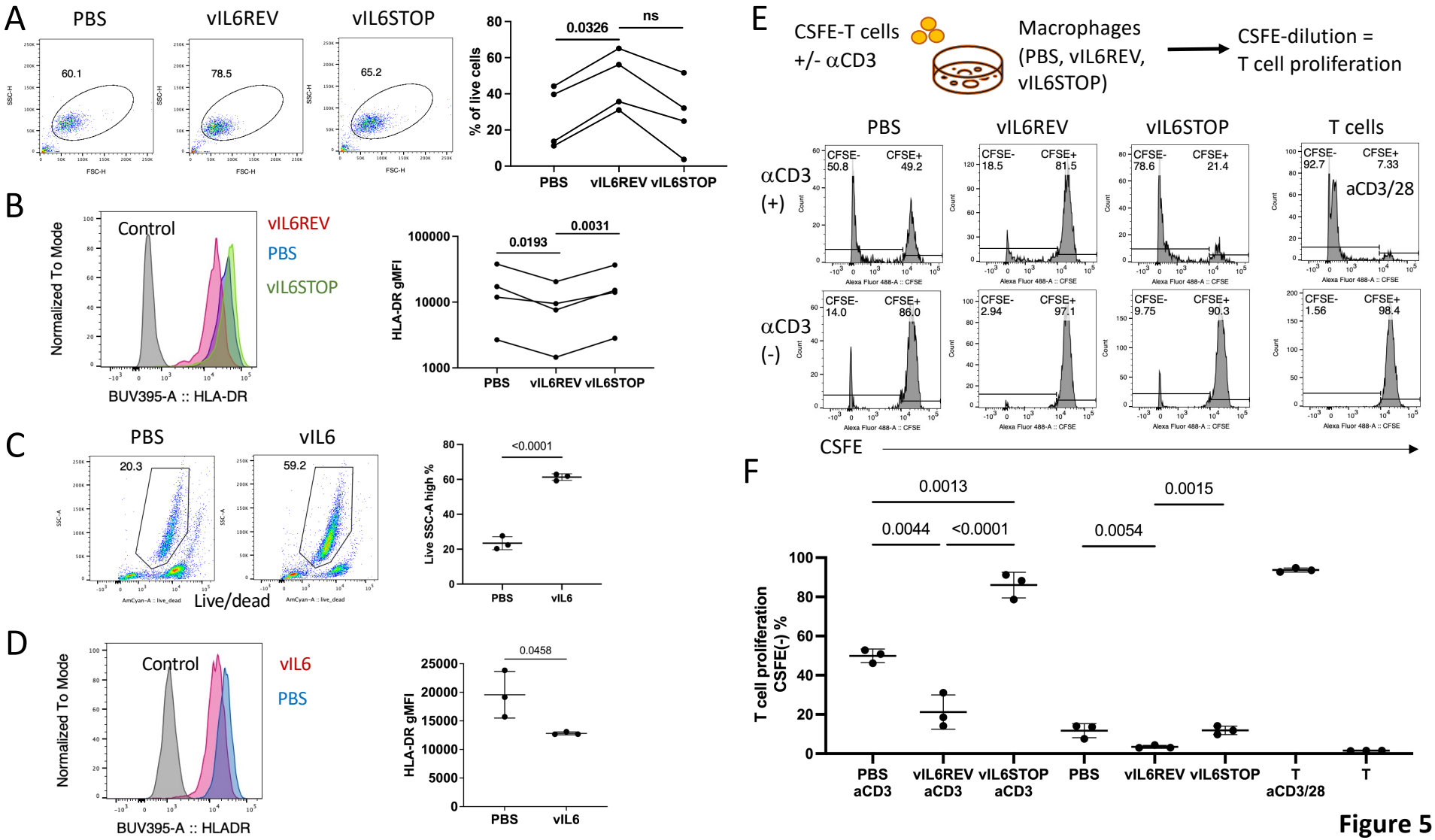
A
PBS
vIL6REV
vIL6STOP
60.1
78.5
65.2
% of live cells
0.0326
ns
PBS
vIL6REV
vIL6STOP
B
Control
vIL6REV
PBS
vIL6STOP
Normalized To Mode
BUV395-A :: HLA-DR
HLA-DR gMFI
0.0193
0.0031
C
PBS
vIL6
20.3
59.2
Live/dead
Live SSC-A high %
<0.0001
D
Control
vIL6
PBS
BUV395-A :: HLADR
0.0458
E
CSFE-T cells
+/- αCD3
Macrophages
(PBS, vIL6REV,
vIL6STOP)
CSFE-dilution =
T cell proliferation
T cells
αCD3
(+)
αCD3
(-)
CFSE-
CFSE+
50.8
49.2
18.5
81.5
78.6
21.4
92.7
7.33
aCD3/28
14.0
86.0
2.94
97.1
9.75
90.3
1.56
98.4
CSFE
F
T cell proliferation
CSFE(-) %
0.0013
0.0044
<0.0001
0.0054
0.0015
PBS
aCD3
vIL6REV
aCD3
vIL6STOP
aCD3
PBS
vIL6REV
vIL6STOP
T
aCD3/28
T

Figure 5

SFig1

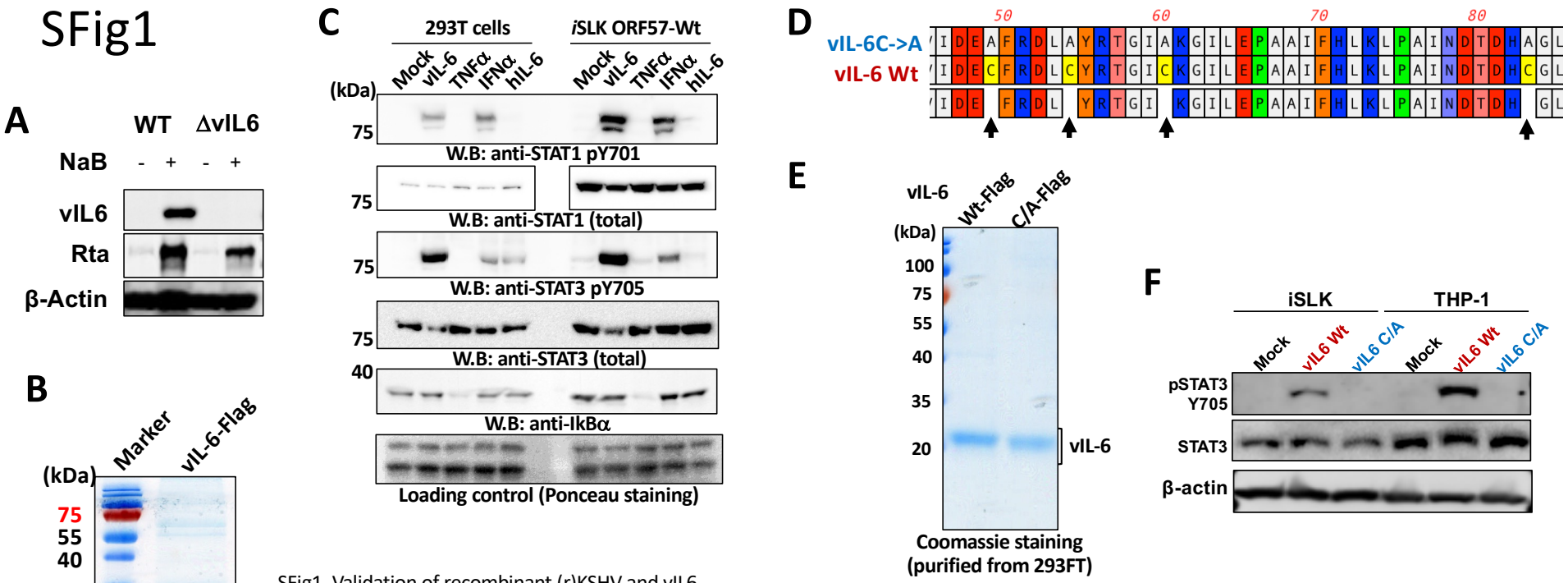

SFig1. Validation of recombinant (r)KSHV and vIL6.
(A) Lack of vIL6 protein expression in vIL6 STOP KSHV producing iSLK cells. iSLK cell lines transduced to express vIL6 of wild type (WT: vIL6 REV) or deficient (ΔvIL6: vIL6 STOP) rKSHV were stimulated with Sodium Butyrate to induce KSHV lytic activation with vIL6 and Rta expression. KSHV-encoded vIL6 and Rta protein, and host β-actin as a control was detected by Western blotting with specific antibodies. (B) Recombinant vIL6-Flag protein was produced in insect cell lines and the purity confirmed by Western blotting with rabbit anti-vIL6 monoclonal antibody. A gel image with molecular weight markers is shown. (C) 293T and iSLK ORF57-wt cell lines were stimulated with 200ng/ml recombinant vIL6 along with controls, TNFα, IFNα, and human (h)IL6, or mock treated. STAT1 and 3 activation was studied by Western blotting with specific antibodies for total STAT1, STAT1 pY701, total STAT3, STAT3 pY705, and IkBα as controls. Ponceau staining for each well are shown as loading control. (D) To validate vIL6 activity, wild type (Wt) or mutant (C->A) are generated. Arrows indicate the location of amino acid residues where mutations are introduced. (E) Wt and C/A mutant vIL6 proteins were expressed in 293FT cell lines, the purity of which confirmed by Western blotting. (F) iSLK and THP-1 cell lines were stimulated with 200ng/ml recombinant Wt or C/A mutant vIL6, or mock treated. STAT3 activation was studied by Western blotting with specific antibodies for total STAT3, STAT3 pY705, and β-actin as controls. Wt but not C/A mutant was able to trigger STAT3 activation.

SFig2

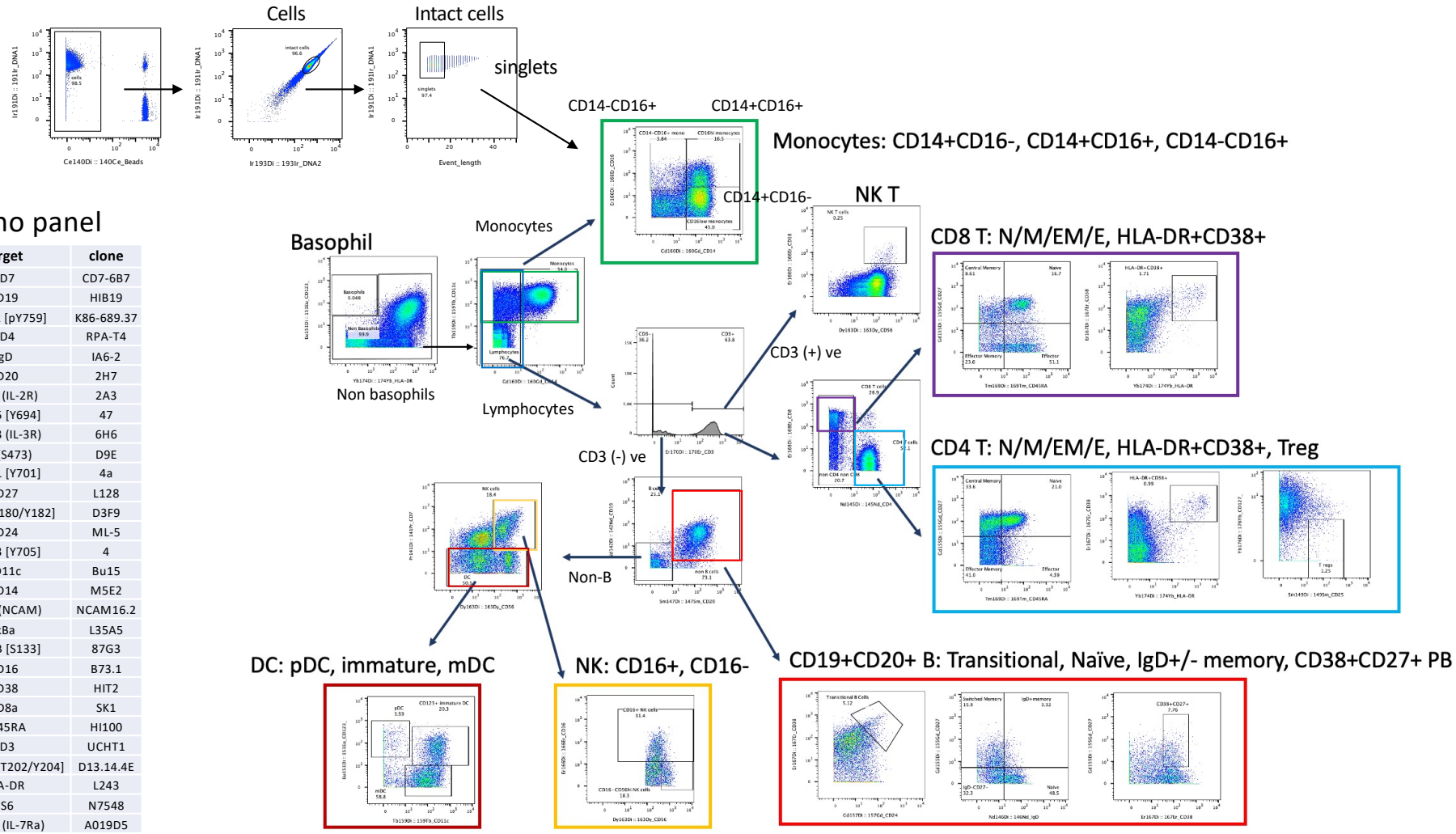

Phospho panel

label	target	clone
141Pr	CD7	CD7-6B7
142Nd	CD19	HIB19
144Nd	pPLCg2 [pY759]	K86-689.37
145Nd	CD4	RPA-T4
146Nd	IgD	IA6-2
147Sm	CD20	2H7
149Sm	CD25 (IL-2R)	2A3
150Nd	pStat5 [Y694]	47
151Eu	CD123 (IL-3R)	6H6
152Sm	Akt (S473)	D9E
153Eu	pStat1 [Y701]	4a
155Gd	CD27	L128
156Gd	p-p38 [T180/Y182]	D3F9
157Gd	CD24	ML-5
158Gd	pStat3 [Y705]	4
159Tb	CD11c	Bu15
160Gd	CD14	M5E2
163Dy	CD56 (NCAM)	NCAM16.2
164Dy	IkBa	L35A5
165Ho	pCREB [S133]	87G3
166Er	CD16	B73.1
167Er	CD38	HIT2
168Er	CD8a	SK1
169Tm	CD45RA	HI100
170Er	CD3	UCHT1
171Yb	pERK 1/2 [T202/Y204]	D13.14.4E
174Yb	HLA-DR	L243
175Lu	pS6	N7548
176Yb	CD127 (IL-7Ra)	A019D5

SFig2. CyTOF phosphor panel and the gating strategy to identify immune cell subsets are shown.

SFig3

A

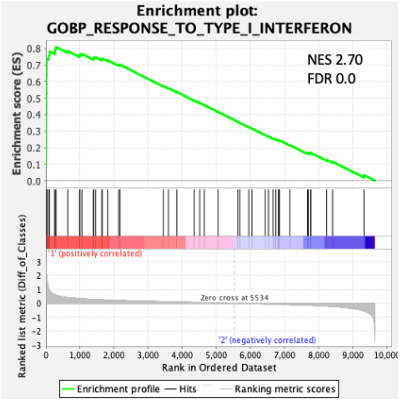

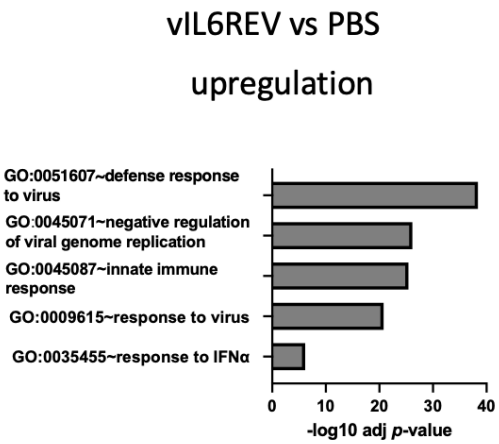

B

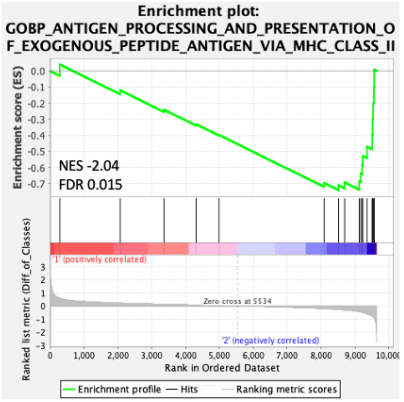

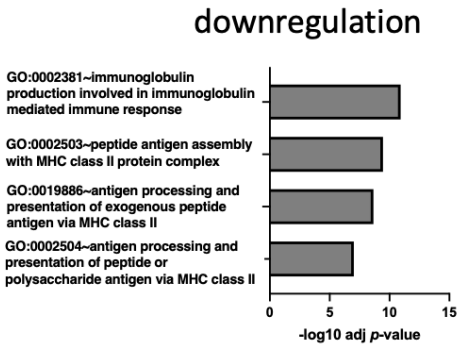

SFig3. Gene Set Enrichment Analysis (GSEA) for vIL6REV-infected vs mock-infected macrophage transcriptomic landscape. The functional enrichment analysis of upregulated genes (A) and downregulated genes (B) in vIL6REV- compared to mock-infected (PBS treated) monocytes. DAVID functional enrichment analysis was performed, and the analysis results of top 5 enriched pathway are shown (Right). The representative results of GSEA are shown (Left).